THE JOURNAL OF PHYSICAL CHEMISTRY B

Article

pubs.acs.org/JPCB

Dye Dynamics in Three-Color FRET Samples

Sören Gehne,[†] Roman Flehr,[†] Andrea Altevogt neé Kienzler,[‡] Maik Berg,[†] Willi Bannwarth,[‡] and Michael U. Kumke*,[†]

[†]Institute of Chemistry (Physical Chemistry), University of Potsdam, Karl-Liebknecht-Str. 24-25, 14476 Potsdam-Golm, Germany

[‡]Institute of Organic Chemistry and Biochemistry, Albert-Ludwigs-University of Freiburg, Albertstr. 21, 79104 Freiburg, Germany

Supporting Information

ABSTRACT: Time-resolved emission data (fluorescence decay and fluorescence depolarization) of two three-color Förster resonance energy transfer (tc-FRET) systems consisting of a carbostyril donor (D), a ruthenium complex (Ru) as relay dye, and a Cy5 derivative (Cy) or, optionally, an anthraquinone quencher (Q) were carefully analyzed using advanced distribution analysis models. Thereby, it is possible to get information on the flexibility and mobility of the chromophores which are bound to double stranded (ds) DNA. Especially the distance distribution based on the analysis of the fluorescence depolarization is an attractive approach to complement data of fluorescence decay time analysis. The distance distributions extracted from the experimental data were in excellent agreement with those determined from accessible volume (AV) simulations. Moreover, the study showed that for tc-FRET systems the combination of dyes emitting on different time scales (e.g., nanoseconds vs microseconds) is highly beneficial in the distribution analysis of time-resolved luminescence data in cases where macromolecules such as DNA are involved. Here, the short lifetimes can yield information on the rotation of the dye molecule itself and the long lifetime can give insight in the overall dynamics of the macromolecule.

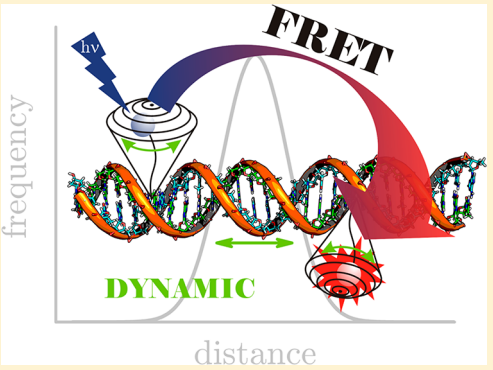

I. INTRODUCTION

Many biological and biochemical events occur on a low nanometer scale and experimental techniques offering a spatial resolution at such dimensions to follow such processes in real time are of utmost importance in many life science applications (e.g., for the investigation of cellular processes). A powerful approach suitable for the study of inter- as well as intramolecular interactions is the so-called Förster resonance energy transfer (FRET).[1−3] The underlying physical principle is a radiationless energy transfer between two fluorophores via dipole−dipole interactions, one acting as energy donor D and a second as acceptor A.[4,5] The transfer efficiency η of FRET depends largely on the intrinsic spectroscopic properties of the dyes (reflected in the Förster distance R_0), on their relative orientation to each other (defined by the orientation factor κ^2), and on the distance R from each other. The distance-dependency of η to R^{-6} make such systems suitable to determine molecular distances typically in the range of 10−100 Å, depending on the particular FRET pair used. As a rule of thumb, the working range is $0.5R_0 < R < 2R_0$. The overall dimensions of macromolecular systems such as proteins or protein clusters can exceed this distance so that the working range of FRET systems has to be enlarged in order to be applicable in the larger systems.[6]

A promising way to achieve this goal and to allow for the investigation of interactions between multiple partners is the combination of two (or more) FRET pairs, which share a so-called relay dye. This chromophore AI acts as an acceptor and a donor for FRET pair one and two, respectively (see Figure 1).

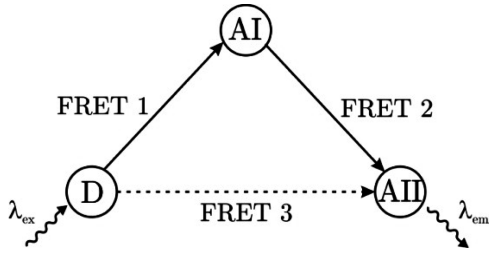

Figure 1. Principle of a three-color FRET system.

Considering the direct energy transfer between the first and the third chromophore, in such a three-color FRET (tc-FRET) system, three energy transfer steps can occur and, hence, the transfer range can be significantly increased.[7−9] Moreover, depending on the combination of individual FRET pairs also the distance resolution can be improved by coupling pairs with one small and one large R_0.

In addition, tc-FRET systems may also allow to determine the position of the three dyes relative to each other and,

Received: June 29, 2012
Revised: August 6, 2012
Published: August 10, 2012

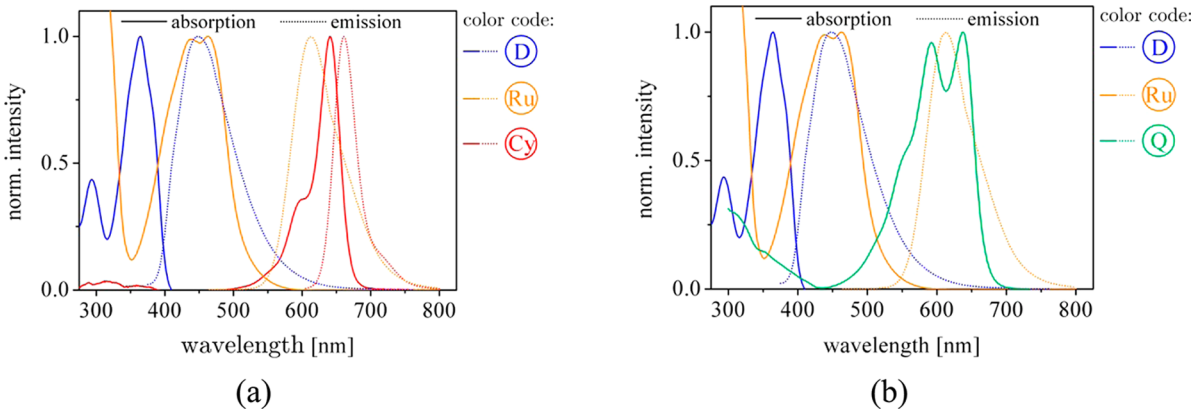

Figure 2. Normalized absorption (solid) and emission (dashed) spectra of the two tc-FRET systems: (a) cyanine dye system D-Ru-Cy and (b) anthraquinone system D-Ru-Q.

subsequently, enable a 3D-spatial resolution yielding an improved capability to monitor folding phenomena or interactions of three molecules in real time.[10,11]

Due to the interdependent requirements for the involved dyes, such systems are difficult to establish. On the one hand, the three dyes need to have well matching spectroscopic properties, and on the other hand, the synthetic challenges for coupling of the dyes to biomolecules have to be met as well.

Recently, we have established two different tc-FRET systems that fulfill these sophisticated requirements.[12,13] Both systems are based on a carbostyril dye (D) as donor in combination with a ruthenium(II)−bathophenanthroline complex (Ru) as first acceptor (AI, see Figure 1), but differ in the acceptor of the second pair, which we have dubbed as AII. In our first reported tc-FRET system we used an anthraquinone derivative (Q) as AII. Due to his nonemitting character, it is possible to measure the undisturbed emission of the Ru(II) complex (relay dye) without contributions from the direct and indirect excitation of acceptor AII. This system was successfully established in oligonucleotides as well as in peptides.[12] In the second tc-FRET system, the anthraquinone was replaced by a cyanine dye, a Cy5 derivative (Cy), and the system was built up with a synthetic oligonucleotide backbone. Here, the occurrence of AII emission is a direct evidence for the successful energy transfer between AI and AII, respectively. Furthermore, it is also an analytical benefit with respect to practical considerations to enlarge the spectral shift between the donor (D) absorption and the "final" emission of AII.[13]

Both tc-FRET systems show an efficient energy transfer due to the large spectral overlap of the carbostyril donor emission and the absorption of the Ru complex as well as for the second transfer step from the Ru complex to the anthraquinone or the cyanine dye (Figure 2).

Another key feature of the tc-FRET systems is the possible selective excitation of each chromophore enabling (i) to specifically analyze each energy transfer step by exciting the corresponding donor and (ii) minimizing direct excitation of AI or AII.[13] From the straightforward analysis of steady-state data, the average interdye distances were determined and were in good accordance with the expected average values obtained from theoretical calculations based on accessible volume (AV) simulations. However, any information on the dynamics of the distance between dyes themselves and biomolecules is averaged out and not resolved by the analysis. However, to use fluorescence probes yielding a maximum of desired information on a system, it is indispensable to be aware of any unwanted intra- and intermolecular interaction that may interfere with the data evaluation.

Time-resolved fluorescence spectroscopy measuring the decay kinetics and the depolarization are powerful techniques to resolve such molecular dynamics. Here, a further benefit of the applied Ru complex, its outstanding long luminescence decay time, which is in the μs range, comes into play. Such luminescence probes with intrinsically long decay times are especially attractive for life science applications because in time-gated detection schemes any interfering background signals limiting the sensitivity can be effectively eliminated. To fully use this potential, a sound interpretation and evaluation of the luminescence decay curves, which are often multiexponential in biological systems due to a distribution of the dyes in different environments, are required. Thus, the distribution in distances between donor and acceptor molecules need to be resolved. In cases where the distribution itself may be time-dependent, the analysis becomes more time-demanding. This might be caused by changes in the relative orientation of the dyes to each other or to the biomolecules they are attached to. Such effects are important to be considered in the data analysis in cases in which the luminescence decay of the dyes is in the same order or longer than molecular motions of the biomolecule.[14]

In the present study, two tc-FRET systems (system 1: carbostyril (D)−ruthenium(II)-bathophenanthroline (Ru)−anthraquinone (Q); and system 2: carbostyril (D)−ruthenium-(II)-bathophenanthroline (Ru)−cyanine dye (Cy)), which have been thoroughly characterized in standard steady-state absorption and emission spectroscopy, the luminescence and depolarization kinetics of the different dyes are analyzed in detail. A major challenge is the evaluation of the multi-exponential decay curves of the Ru-luminescence in the presence of an acceptor. In the present work a unique analysis of data from complementary experimental approaches (time-resolved fluorescence and time-resolved depolarization) in combination with theoretical models is carried out to resolve the distance distributions for the two tc-FRET systems.

II. EXPERIMENTAL SECTION

II.1. Sample Preparation. The synthesis of the different DNA samples is described in detail elsewhere.[12,13] The tc-FRET systems based on double-stranded DNA (ds-DNA) were formed by hybridizing a Ru complex containing oligonucleotide to the complementary one, which was either functionalized with D and Cy or with D and Q (see Figures 3 and 4). Two three-color FRET (tc-FRET) systems of

dx.doi.org/10.1021/jp3064273 | J. Phys. Chem. B 2012, 116, 10798−10806

A1 5′ACT ATT ATC TAT GTA AAT TCT CTA CTA TTC 3′

A2 5′ACT ATT ATC TAT GTA AAT TCT CTA CT^{D}A TTC 3′

A3 5′ACT ATT ATC TAT GTA AAT TCT^{D} CTA CTA TTC 3′

A4 5′ACT AT^{Cy}T ATC TAT GTA AAT TCT CTA CTA TTC 3′

A5 5′ACT ATT ATC T^{Cy}AT GTA AAT TCT CTA CTA TTC 3′

A6 5′ACT AT^{Q}T ATC TAT GTA AAT TCT CTA CTA TTC 3′

A7 5′ACT ATT ATC T^{Q}AT GTA AAT TCT CTA CTA TTC 3′

A8 5′ACT AT^{Cy}T ATC TAT GTA AAT TCT^{D} CTA CTA TTC 3′

A9 5′ACT ATT ATC T^{Cy}AT GTA AAT TCT^{D} CTA CTA TTC 3′

A10 5′ACT AT^{Cy}T ATC TAT GTA AAT TCT CTA CT^{D}A TTC 3′

A11 5′ACT ATT ATC T^{Cy}AT GTA AAT TCT CTA CT^{D}A TTC 3′

A12 5′ACT AT^{Q}T ATC TAT GTA AAT TCT^{D} CTA CTA TTC 3′

A13 5′ACT ATT ATC T^{Q}AT GTA AAT TCT^{D} CTA CTA TTC 3′

A14 5′ACT AT^{Q}T ATC TAT GTA AAT TCT CTA CT^{D}A TTC 3′

A15 5′ACT ATT ATC T^{Q}AT GTA AAT TCT CTA CT^{D}A TTC 3′

B1 5′GAA TAG TAG AGA ATT TAC ATA GAT AAT AGT 3′

B2 5′GAA TAG TAG AGA ATT^{Ru} TAC ATA GAT AAT AGT 3′

Figure 3. Sequences of oligonucleotides (**A1**−**A15**) and their complementary oligonucleotides (**B1** and **B2**).

each type were analyzed, differing in the second acceptor AII (Cy or Q, respectively). For both systems, two relative distances between the dyes of each FRET pair were investigated. While the position of the Ru complex was fixed in the middle of the ds-DNA, the positions of the other dyes (D and Cy or Q, see Figure 3) was varied and referred to by the subscripts "1" and "2", respectively. Here, "1" denotes the nearest and "2" the largest distance relative to the Ru complex. By combining the oligonucleotides, it was possible to create the different tc-FRET systems and reference samples. These reference samples contained either one or two chromophores only and were used to characterize the single transfer steps in detail, especially the direct energy transfer between D and Cy or Q, respectively.[12,13]

II.2. Photophysical Characterization. The absorption and emission measurements were carried out using a Cary 500 UV/vis spectrometer (Varian) and a Fluoromax3 fluorescence spectrometer (Jobin Yvon), respectively.

For the time-resolved emission measurements, a FL920 fluorescence lifetime spectrometer (Edinburgh Instruments) operated in the time-correlated single-photon-counting (TCSPC) mode was used. The carbostyril donor (D) was excited by a picosecond pulsed laser diode EPL-375 (Edinburgh Instruments) at λ_{ex} = 375 nm and a repetition rate of 5 MHz. For the excitation of the Ru complex, the frequency-doubled output (second harmonic generation (SHG); vertical polarization) of a Titan sapphire laser (Tsunami 3960, Spectra Physics; λ_{TiSa} = 860 nm, λ_{SHG} = 430 nm, pulse width (fwhm) 120 fs) was applied. The repetition rate was reduced from 80.2 MHz to 50 kHz by a Pulse Picker (Pulse Select, APE). The cyanine dye (Cy) was excited using a supercontinuum laser source (SC-400-PP, Fianium) at λ_{ex} = 590 nm, with the repetition rate set to 20 MHz. The detection of the luminescence was performed in a right-angle configuration relative to the incoming beam using a multichannel plate (ELDI EM1−132/300; Europhoton GmbH). The emission polarizer was set to magic angle conditions (54.7°) to avoid anisotropy artifacts in the measured luminescence decay curves. For the time-resolved anisotropy measurements the fluorescence decays were recorded with vertical polarized excitation light and emission polarizers, set in a vertical ($I_{VV}(t)$) and horizontal ($I_{VH}(t)$) position. The subscripts V (vertical) and H (horizontal) denote the orientations of the polarizers in the excitation and emission beam, respectively. The anisotropy decay $r(t)$ was calculated according to eq 1[15] and the G-factor was determined by fitting the synthesized fluorescence decay curve $I_{VV}(t) + 2{\cdot}G{\cdot}\ I_{VH}(t)$.[16]

$$r(t) = \frac{I_{VV}(t) - GI_{VH}(t)}{I_{VV}(t) + 2GI_{VH}(t)} \tag{1}$$

Here, I is the luminescence intensity at a given polarizer configurations (V, vertical; H, horizontal) and G is the instrumental correction factor (see eq 2).

$$G = \frac{I_{HV}}{I_{HH}} \tag{2}$$

II.3. Data Analysis. *II.3.1. Distance Determination.* The FRET efficiency η is calculated according to eq 3, where I_D (τ_D) is the luminescence intensity (decay time) of the donor in the absence and I_{DA} (τ_{DA}) in the presence of an acceptor.

$$\eta = 1 - \frac{I_{DA}}{I_D} = 1 - \frac{\tau_{DA}}{\tau_D} \tag{3}$$

Based on the FRET theory, the distance R between donor and acceptor can be calculated by the transfer efficiency η. This is shown in eq 4:

$$\eta = \frac{R_0^6}{R_0^6 + R^6} \leftrightarrow r = R_0\left[\frac{1}{\eta} - 1\right]^{1/6} \tag{4}$$

Here, the key parameter is the Förster distance, R_0, which is specific for a given FRET pair (see eq 5). R_0 can be calculated from the spectroscopic properties of the involved dyes (Φ_D, quantum yield of the donor; f_D (λ), area normalized donor emission spectra; ε_A (λ), extinction coefficient spectra of the acceptor), the orientation factor κ^2 (orientation of the transition dipoles of donor and acceptor relative to each other), and the refractive index n of the solvent (eq 5):[17,18]

$$R_0^6 = \Phi_D\kappa^2\left(\frac{9(\ln 10)}{128\pi^5 N_A n^4}\right)\int_0^\infty f_D(\lambda)\varepsilon_A(\lambda)\lambda^4 d\lambda \tag{5}$$

Furthermore, N_A denotes Avogadro's number and λ is the wavelength (in nm).

To compare a distance distribution with another one, it is advisable to determine the expected distance μ and the standard deviation σ according to eqs 6 and 7, respectively:[19]

$$\mu = \int_{-\infty}^{+\infty} R{\cdot}P(R)dR \tag{6}$$

$$\sigma^2 = \int_{-\infty}^{+\infty} (R-\mu)^2{\cdot}P(R)dR \tag{7}$$

Here, $P(R)$ denotes the probability of the distance R between donor and acceptor. In the case of a symmetric distance distribution, e.g. the Gaussian function, the expected distance equals the modal value Ω_{max}. This is not true for an asymmetric distribution, for which the expected

dx.doi.org/10.1021/jp3064273 | J. Phys. Chem. B 2012, 116, 10798−10806

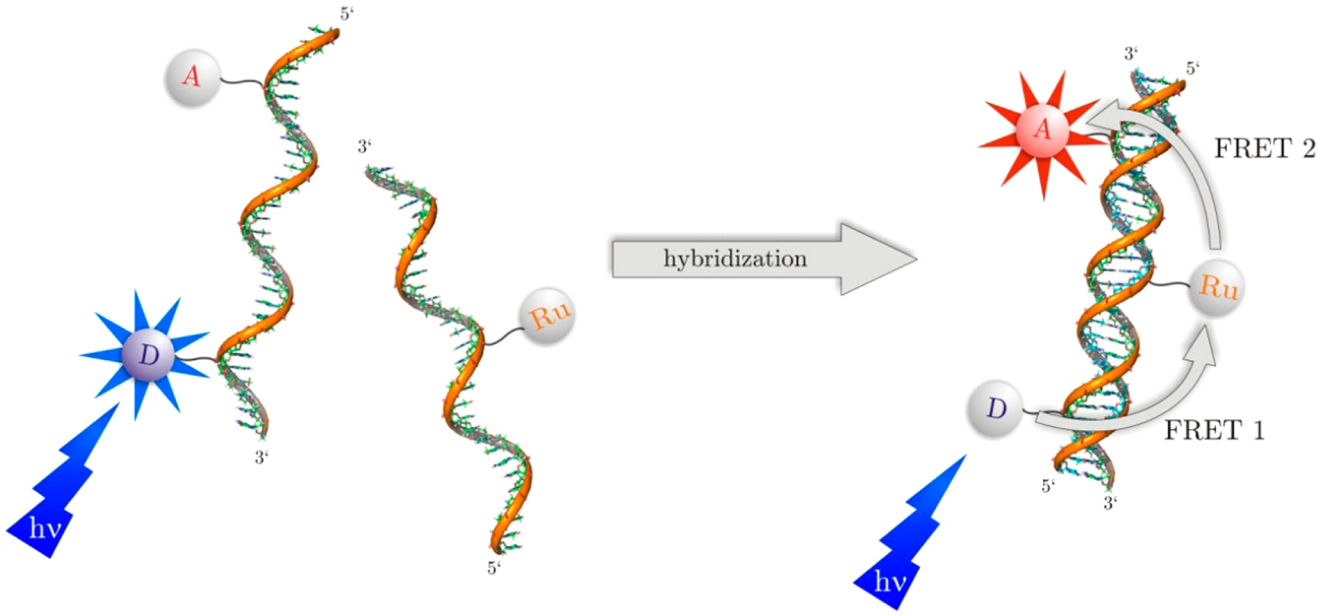

Figure 4. Schematic representation of the tc-FRET system based on double-stranded DNA. Only after hybridization the different energy transfers were active (A = Q or Cy).

distance can be smaller or larger than Ω_{max} depending on the asymmetry.

II.3.2. Anisotropy Decay. The coupling of a dye to a DNA double strand (ds-DNA) can result in a change in its photophysical properties such as an alteration in the luminescence decay time as well as in the rotational correlation time.[20−24] In the present study the dyes are coupled by a flexible spacer to the DNA strands. For such systems the "wobble-in-a-cone" model may be used in the analysis of the time-resolved anisotropy $r(t)$, according to eq 8:[16]

$$r(t) = (r_0 - r_\infty)\exp\left\{-\frac{t}{\varphi}\right\} + r_\infty \tag{8}$$

Here, r_0 is the fundamental anisotropy, r_∞ is the limiting anisotropy, and φ denotes the rotational correlation time. The parameter A_∞ describes the extent of motional restriction and can be calculated based on eq 9 with the semicone angle θ_c .

$$A_\infty = \frac{r_\infty}{r_0} = \left[\frac{1}{2}\cos\theta_c(1 + \cos\theta_c)\right]^2 \tag{9}$$

In addition to the fast (but restricted) motion of the dye itself, the overall rotation of the ds-DNA has to be considered. In that case, the time-resolved anisotropy is given by a product of both rotational motions (see eq 10):[15]

$$r(t) = \left[(r_0 - r_\infty)\exp\left\{-\frac{t}{\varphi_{seg}}\right\} + r_\infty\right]\exp\left\{-\frac{t}{\varphi_{DNA}}\right\} \tag{10}$$

At this, φ_{seg} and φ_{DNA} represent the rotational correlation times for the restricted rotation of the dye and for the overall rotation of the ds-DNA, respectively.

II.4. Theoretical Calculation. Accessible volume (AV) simulations based on the "Model Satelite Prior" algorithm were carried out with the program *FRETnpsTools* to calculate theoretical interdye distances.[25−27] The required pdb-file of the double-stranded DNA was generated with the *Nucleic Acid Builder* software, which is a part of the software package *AmberTools*.[28]

III. RESULTS AND DISCUSSION

Based on the steady-state luminescence data (shown in a previous publication)[13] the average distances between the different dyes were determined and were in good accordance with the theoretical average distances.[12,13] However, from the steady-state data, no information on the flexibility of the dyes when attached to ds-DNA is accessible. Moreover, in the case of the Ru-Cy FRET pair, the evaluation of the steady-state data is difficult due to the fact that the emission spectra of both compounds show a distinct spectral overlap. Here, the analysis of time-resolved fluorescence data can help to overcome these shortcomings. Especially, to gain detailed information on dynamic processes and on the mobility of the dyes, time-resolved luminescence measurements, luminescence decay kinetics, as well as time-resolved depolarization, are powerful tools. In the special case of Ru and Cy as donor−acceptor pair, the distinctly different decay times of the two dyes will allow to discriminate the luminescence contributions of both and yield a precise calculation of the interdye distance.

III.1. Distance Determination Based on Luminescence Decay Times. In Figure 5 the fluorescence decays of the

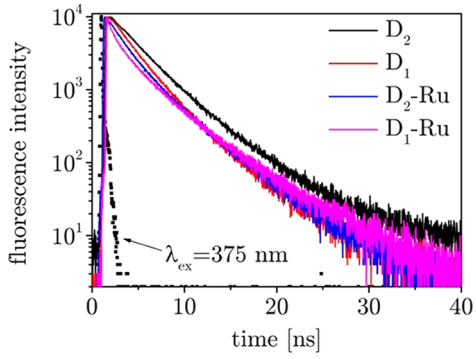

Figure 5. Fluorescence decay curves of the carbostyril donor (D) in absence and in presence of the Ru complex (Ru; λ_{ex} = 375 nm, λ_{em} = 440 nm). D_1 and D_2 (sample no. **A3/B1** and **A2/B1**) refer to the carbostyril labeled-only samples and D1-Ru and D2-Ru (sample no. **A3/B2** and **A2/B2**) refer to the regular two-color FRET reference samples.

dx.doi.org/10.1021/jp3064273 | J. Phys. Chem. B 2012, 116, 10798−10806

Table 1. FRET Efficiencies and Interdye Distances Based on Emission Intensity (R_s) and Decay Time (R_t) Data of the First Energy Transfer Step D-Ru Compared with Theoretical Values (R_{theo})

sample no.	sample	$\eta_{D\text{-}Ru,t}$	$R_{D\text{-}Ru,theo}$ [a] (nm)	$R_{D\text{-}Ru,s}$ [b,c] (nm)	$R_{D\text{-}Ru,t}$ [b] (nm)
A2/B2	D_2-Ru	0.24 ± 0.03	4.6 ± 0.7	4.7 ± 0.5	4.6 ± 0.1
A3/B2	D_1-Ru	0.49 ± 0.06	3.5 ± 0.5	3.8 ± 0.3	3.9 ± 0.2
A8/B2	D_1-Ru-Cy_2	0.49 ± 0.06	3.5 ± 0.5	3.7 ± 0.2	3.8 ± 0.2
A9/B2	D_1-Ru-Cy_1	0.48 ± 0.06	3.5 ± 0.5	4.0 ± 0.5	3.9 ± 0.2
A10/B2	D_2-Ru-Cy_2	0.25 ± 0.03	4.6 ± 0.7	4.7 ± 0.4	4.6 ± 0.1
A11/B2	D_2-Ru-Cy_1	0.25 ± 0.03	4.6 ± 0.7	4.5 ± 0.1	4.6 ± 0.1

[a]Calculated from AV-simulations. [b]With R_0(D-Ru) = 38.2 Å. [c]From ref 12 and 13.

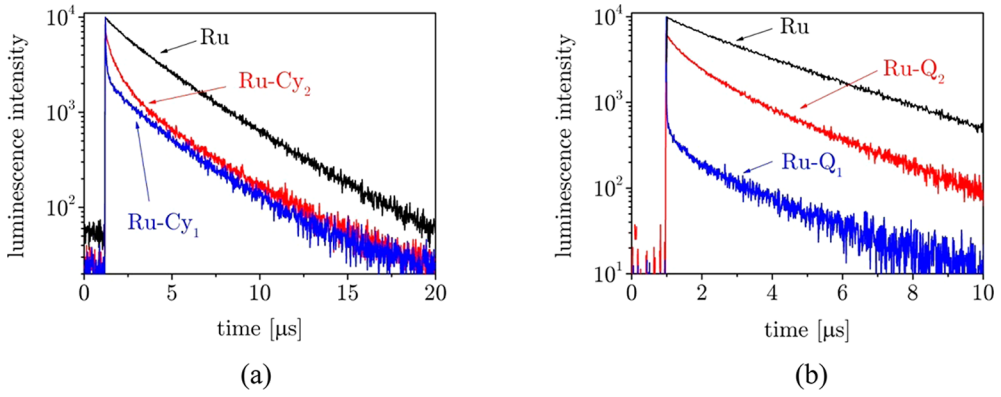

Figure 6. Luminescence decay curves of the Ru complex in the absence (Ru, sample no. **A1/B2**) and presence of (a) Cy and (b) the anthraquinone quencher Q (λ_{ex} = 430 nm, λ_{em} = 615 nm; sample (sample nos.) (a) Ru-Cy_2 (**A4/B2**) and Ru-Cy_1 (**A5/B2**), (b) Ru-Q_2 (**A6/B2**) and Ru-Q_1 (**A7/B2**), respectively).

carbostyril (D) coupled to ds-DNA at different positions in the absence (reference samples) and presence of the Ru complex are shown. It can be seen that (i) the fluorescence decay time of D was slightly dependent on its relative position on the DNA strand which might be due to the close proximity of either one or two guanine bases (on the cDNA strand) resulting in an additional quenching[12,29] and (ii) in the presence of Ru the fluorescence decay was increased.

The carbostyril showed a fast fluorescence decay on the lower nanosecond scale that was evaluated using a biexponential decay kinetic. The mean decay time of D in position 2 decreased from τ_{D_2} = 3.3 ns to $\tau_{D_2\text{-}Ru}$ = 2.5 ns, and from τ_{D_1} = 2.7 ns to $\tau_{D_1\text{-}Ru}$ = 1.4 ns in position 1 (see Figure 5 and Table SI1). The corresponding fluorescence decay times of the carbostyril donor in the absence and in the presence of the Ru complex were used to calculate the energy transfer efficiency $\eta_{D\text{-}Ru,t}$ (see Table 1). FRET efficiencies of about 25% for D_2-Ru and of about 50% for D_1-Ru were determined, and subsequently, the average distance R between Ru and D was calculated ($R_{D_2\text{-}Ru,t}$ = (4.6 ± 0.1) nm and $R_{D_1\text{-}Ru,t}$ = (3.9 ± 0.2) nm, respectively). In general, the results are in good agreement with the mean distances $R_{D\text{-}Ru,theo}$ obtained from AV simulations as well as the distances $R_{D\text{-}Ru,s}$ calculated from the decrease of the luminescence intensity (see Table 1).

While the evaluation of the first energy transfer step between carbostyril and Ru complex based on the fluorescence decays is possible by a robust approach using the average fluorescence decay times, the analysis of the Ru complex as donor in the second energy transfer step is more complex. In contrast to carbostyril, the longer luminescence decay is more prone to influences resulting from molecular motions. In turn, the proper analysis of the luminescence decay can shed light on dynamic processes involving the motion of the dye molecules attached to the ds-DNA.

In Figure 6a the luminescence decay curves of the Ru complex in absence and presence of Cy for direct excitation at λ_{ex} = 430 nm are shown. Due to the energy transfer to Cy the luminescence decay of Ru increased. The overall increase was depending on the relative position of Cy along the ds-DNA but for both distances a small amount of Ru remains unquenched due to incomplete hybridization or a failed labeling of the single stranded DNA. Moreover, from the experimental data it can be seen that also the overall time-dependence of the Ru luminescence was altered and is no longer represented by a simple first order decay law. This change in the Ru luminescence time dependence was found in the presence of Cy as well as of Q as acceptor (see Figure 6a,b). The observed complex decay kinetics can be seen as a consequence of (i) the relatively long Ru luminescence decay time (τ_{Ru} ~ 3.0 μs) and (ii) the flexibility of the spacer that attaches the dyes to the ds-DNA. The combination of both factors can lead to a dynamic distribution of distances between donor (Ru) and acceptor (Cy or Q), consequently, also of the FRET efficiencies. For the pair Ru-Cy the effect of linker mobility on the FRET parameters was much more pronounced than in the case of D-Ru. In the latter case, the much shorter fluorescence decay time of D (only a few ns, vide supra) attenuated the time-dependent influence of molecular motions on the observed FRET efficiency. To extract additional information on the motion of the Ru dye, an advanced data analysis was applied (see eq 11). A distribution function was implemented to consider the dynamics in the distances between Ru and Cy (or Q, respectively). In eq 11, $P(R)$ represents the distribution function considering the donor–acceptor distances.

dx.doi.org/10.1021/jp3064273 | J. Phys. Chem. B 2012, 116, 10798–10806

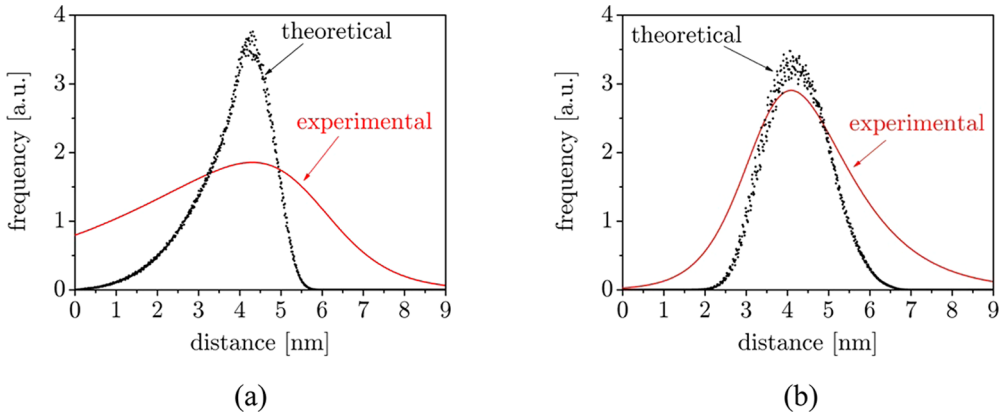

Figure 7. Comparison of theoretical (black dots) and experimental (red line) derived interdye distance distributions for the samples (sample no.) (a) Ru-Cy_1 (**A5/B2**) and (b) Ru-Cy_2 (**A4/B2**).

$$I_{\text{Ru-A}}(t) = I_{\text{Ru-A}}(0)\int_0^\infty P(R)\exp\left\{-\frac{t}{\tau_{\text{Ru}}} - \frac{t}{\tau_{\text{Ru}}}\left(\frac{R_0}{R}\right)^6\right\}$$

$$\text{with A} = \text{Cy or Q} \qquad (11)$$

For sufficiently long linker lengths, the distance distribution between donor and acceptor can be approximated to be of the Gaussian type.[17] On the other hand, for short linkers, the diffusion of the chromophore can be additionally influenced by heterogeneities as well as the structure of the ds-DNA, so that there are regimes in the accessible volume the dye moieties arrive more easily than other areas. Accordingly, the distance distribution is no longer symmetric and is better described by an asymmetric distribution function, for example, an asymmetric double-sigmoidal (ADS) function (see eq 12).

$$P(R) = \frac{1}{1+\exp\left\{-\frac{R-\Omega_{\max}+\frac{w_1}{2}}{w_2}\right\}}\left[\frac{1}{1+\exp\left\{-\frac{R-\Omega_{\max}-\frac{w_1}{2}}{w_3}\right\}}\right] \qquad (12)$$

$\Omega_{\max}$ denotes the modal value, w_1 specifies the frequency of the modal value, and w_2 and w_3 describe the shape of the distance distribution at short and long distances (measure of asymmetry), respectively.

The experimental data were analyzed using the combination of eqs 11 and 12 and from the analysis of these values the distribution parameters were obtained. Figure 7 shows the calculated distance distributions between Ru and Cy based on the luminescence decay data in comparison with the distance distributions obtained from AV simulations.

The experimental and theoretical distance distributions were in good agreement with respect to the expected distance μ (calculated according to eq 6), but distinct differences were found in the width of the distributions (for both distances of the acceptor Cy relative to the Ru donor). Here, the width of the experimental distributions was larger. This was a consequence of the trade off necessary to accept measuring samples in which the contributing luminescence decay times cover the time range between several ns and a few μs (see Figure 6), for example, the short component of the luminescence decay ($t \leq 500$ ns after excitation) has to be fit with high accuracy for the exact determination of the small donor–acceptor distances. For the sample Ru-Cy_1, the data analysis of the short decay component was less precise due to the small number of data points used in the data fitting at short times compared to the overall detection window of 20 μs (see Figure 6). Accordingly, the distance distribution will broaden toward small distances. To quantify these findings, the expected distance μ and the standard deviation σ of the distance distributions was calculated according to eqs 6 and 7, respectively (see Table 2, as well as Figure 7 and Figure SI1).

Table 2. Interdye Distances of the Second Energy Transfer Steps Ru-Cy and Ru-Q Calculated from Emission Intensity (R_s) and Decay Time (R_t) Data Compared with Theoretical Values (R_{theo})[a]

		$R_{\text{Ru-A,theo}}$[b,c] (nm)		$R_{\text{Ru-A,t}}$[b,d] (nm)		
sample no.	sample	μ	σ	μ	σ	$R_{\text{Ru-A,s}}$[b,d,e] (nm)
A4/B2	Ru-Cy_2	4.3	0.8	4.6	1.7	5.0 ± 0.2
A5/B2	Ru-Cy_1	3.8	0.9	3.8	2.0	4.4 ± 0.2
A6/B2	Ru-Q_2	4.1	0.7	3.9	1.5	3.8 ± 0.4
A7/B2	Ru-Q_1	3.5	0.5	3.5	1.4	3.2 ± 0.3
A8/B2	D_1-Ru-Cy_2	4.3	0.8	4.3	1.4	4.9 ± 0.2
A9/B2	D_1-Ru-Cy_1	3.8	0.9	4.0	2.3	4.5 ± 0.2
A10/B2	D_2-Ru-Cy_2	4.3	0.8	4.5	1.2	4.8 ± 0.2
A11/B2	D_2-Ru-Cy_1	3.8	0.9	4.1	1.9	4.7 ± 0.2
A12/B2	D_1-Ru-Q_2	4.1	0.7	4.3	2.0	3.7 ± 0.4
A13/B2	D_1-Ru-Q_1	3.5	0.5			3.3 ± 0.3
A14/B2	D_2-Ru-Q_2	4.1	0.7			4.1 ± 0.4
A15/B2	D_2-Ru-Q_1	3.5	0.5	3.7	1.4	3.5 ± 0.3

[a]Here R_s is shown with errors, while R_t and R_{theo} are specified by the standard deviation σ of the distance distribution, which contains information about the systems dynamic. [b]With A = Cy or Q. [c]Calculated from AV-simulations. [d]With R_0(Ru-Cy) = 50.0 Å; R_0(Ru-Q) = 32.0 Å. [e]From ref 12 and 13.

In Table 2 and in Figure 8 the results obtained from the different data evaluations are compared. For the Ru-Q pair a good agreement between the results obtained from steady-state as well as time-resolved data and AV-simulation was found. Moreover, by analyzing the luminescence decay kinetics not only the average Ru-Q distance were determined but also information on the distribution of distances due to intramolecular motions of the dye-linker part becomes accessible (e.g., see bars in Figure 8). For Ru-Cy, the distances obtained

dx.doi.org/10.1021/jp3064273 | J. Phys. Chem. B 2012, 116, 10798–10806

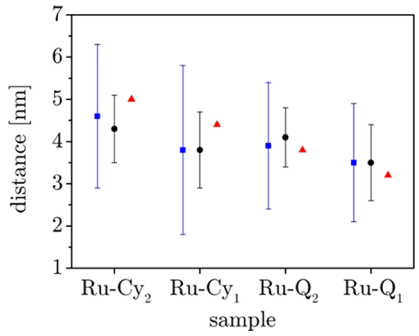

Figure 8. Comparison of theoretical (black circles) and experimental (blue squares) derived interdye distances with standard deviations resulting from distance distributions with that distances resulting from steady-state data (red triangles). With the latter method no information about mobility is available (hence, no bars are shown).

from the analysis of the time-resolved data are in better agreement with the AV-simulations than the distances based on the steady-state emission data, because of less distortion of the decay data due to the spectral overlap of the emission spectra of both dyes. The time-resolved data were recorded at an emission wavelength of λ_{em} = 615 nm where the emission of Cy is small. A further benefit is the fact that the luminescence decay times of Ru and the directly excited Cy are very different (μs and ns, respectively), hence, allowing a good separation of signals of both dyes (due to the combination of good spectral as well as temporal separation; see Table 2 and Figure 8). This is a major advantage in the use of the thermodynamically and kinetically very stable Ru complex to be applicable in time-resolved detection schemes.

III.2. Distance Determination Based on Depolarization Measurements. In complementary experiments, the time-resolved depolarization of D and Cy attached to ds-DNA was measured and the anisotropy was calculated according to eq 1. The time-dependence of the anisotropy is indicative of molecular motions and reflects the degree of hindrance in mobility of the dye molecules. The anisotropy decays for D and Cy attached at different locations along the ds-DNA are shown is Figure 9. In a previous publication we reported on the restriction of the motion of D due to the attachment to the ds-DNA in view of the validity of $\kappa^2 = 2/3$; this assumption is only true for free rotating dyes.[20] The rotational correlation time of free and ds-DNA-bound D was comparable. It is expected that the hindrance in mobility of dyes attached to ds-DNA is determined by the linker rigidity and length as well as the depth and width of the grooves of ds-DNA. The influence of dye linker length and the groove shape on the anisotropy of a Cy5 was reported by Seidel et al.[22] Here, the depolarization of D and Cy is analyzed by more sophisticated models to get more detailed information on the extent of motional restriction.

The depolarization of the Ru luminescence could not be determined because of the large difference between luminescence decay time on the one hand side and the time constants of rotational motion of the dye involved (ns motion vs μs luminescence decay time), which limits the extraction of meaningful information from depolarization measurements.

The anisotropy decay $r(t)$ of the free dyes (D and Cy, respectively) can be well described by a single rotational correlation time φ. Due to the coupling of the dyes to the ds-DNA, the anisotropy decay was significantly altered: the decrease of the anisotropy (i) became slower and (ii) is no longer described by a single rotational motion. In the data evaluation, the coupling of a fast rotational motion of the dye to the slow movement of the ds-DNA as well as a possible hindrance of the dye motion due to the proximity to the ds-DNA has to be considered. An established model to describe the rotational motions in such macromolecular systems is the *wobble-in-a-cone* model (see eq 8). The additional rotational motion of the ds-DNA is considered by an extra rotational component described by the rotational correlation time φ_{DNA} (see eq 10). The parameter A_∞ describes the restriction of the dye motion to a conical volume and allows calculating the semicone angle θ_c based on eq 9. For the investigated dye-ds-DNA systems, this semicone angle was found to be in the range between 19 and 36°, depending on the dye and its position along the ds-DNA (see Table 3). From the data it can already be concluded that the dyes mobility relative to the ds-DNA is restricted, for example, due to localization in the grooves of the ds-DNA.[22] The rotational motion of the dyes themselves was not altered significantly considering the uncertainty of the determined values of 0.2 ns. The rotational correlation times ϕ of approximately 0.3 and 0.8 ns of the free dyes changed to 0.6 and 0.7 ns (φ_{seg} in Table 3) for D and Cy bound to ds-DNA, respectively (see Table 3).

To complement the considerations of molecular motion and its effect on the observed FRET, the time-resolved anisotropy data (e.g., the cone angles θ_c) were also used to calculate a distance distribution between D and Cy.

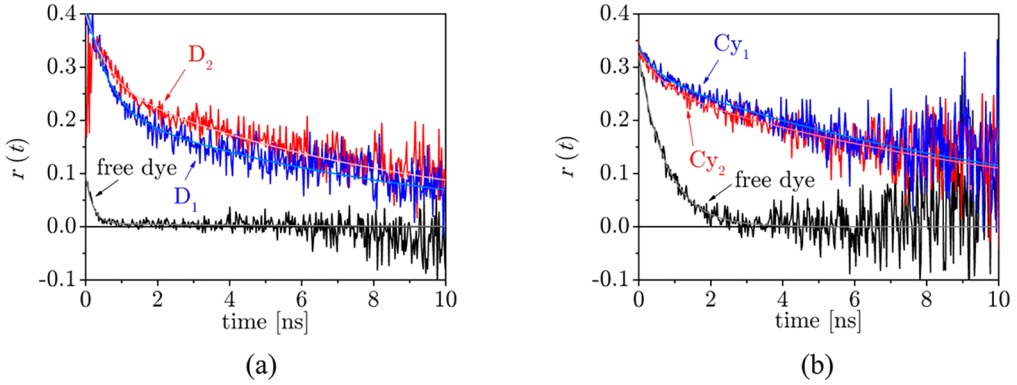

Figure 9. Comparison of the anisotropy decays (shown with corresponding fit curve) of the free dyes (a) D and (b) Cy compared with those from the dyes attached to the ds-DNA (a) D_1 and D_2 (sample nos. **A3/B1** and **A2/B1**) and (b) Cy_1 and Cy_2 (sample nos. **A5/B1** and **A4/B1**), respectively.

dx.doi.org/10.1021/jp3064273 | J. Phys. Chem. B 2012, 116, 10798−10806

Table 3. Parameters Obtained by Analyzing the Anisotropy Decay Data with the Corresponding Models

free dye: single rotational correlation time					
sample		φ (ns)		r_0	
D		0.3 ± 0.2		0.09 ± 0.05	
Cy		0.8 ± 0.2		0.32 ± 0.03	
ds-DNA bound dye: *wobble-in-a-cone* model with respect to ds-DNA rotation					
sample no.	sample	φ_{seg} (ns)	φ_{DNA} (ns)	A_∞	θ_c
A2/B1	D_2	0.7 ± 0.1	8.8 ± 1.4	0.68 ± 0.10	(29 ± 4)°
A3/B1	D_1	0.6 ± 0.2	8.5 ± 1.3	0.51 ± 0.08	(36 ± 3)°
A4/B1	Cy_2	0.7 ± 0.2	11.5 ± 0.5	0.80 ± 0.13	(22 ± 5)°
A5/B1	Cy_1	0.6 ± 0.1	10.9 ± 0.4	0.85 ± 0.13	(19 ± 6)°

Based on the equation introduced by Clegg et al., the overall dimensions of the ds-DNA were calculated (vide infra).[30,31] In Figure 10, a rough scheme of a ds-DNA rod and two attached dyes with their corresponding rotational cone determined from the time-resolved depolarization measurements is depicted.

For D and Cy based on the anisotropy data cones are defined that represent the accessible space for the dye molecule linked to the ds-DNA. The relative orientation of the cones to each other is dependent on the number of separating base pairs (Δbp). The turn of the helix and the subsequent relative angle between the two dyes is determined on the basis of a B-form ds-DNA helix in solution: radius 1 nm, rise of 0.34 nm, and turn of 36° per base pair. Assuming a stiff linker between dye and ds-DNA with the length l_{link}, it is possible to calculate the coordinates the dye moieties can reach on the surface of the spherical segment defined by the cone (see Figure 10). For the calculation of the distance distributions, the number of points on the cone surface segment was assumed to be equal for both dyes. About 1000 points were arranged equidistantly on the segment surface, yielding roughly 1 mill. distances between the points on each surface.[32,33]

The calculated interdye distance distributions between D and Cy obtained from the evaluation of the anisotropy data were compared with the distance distributions arising from AV simulations (see Figure 11).

When comparing the distributions, those determined by anisotropy measurements are narrower but the calculated values of the mean distance μ are in good agreement (see Table 4). The smaller width σ of the distribution is due to the assumption of the stiff linker. Considering a totally flexible linker, the dye moieties can reach positions beyond as well as inside this restricted volume and therefore the interdye distance distribution should become broader.

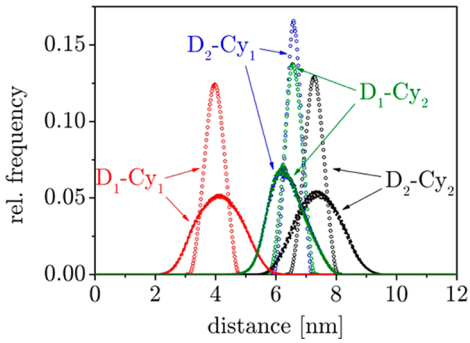

Figure 11. Comparison of theoretical (closed circles) derived interdye distance distributions with those resulting from analyzing anisotropy data (open circles).

Table 4. Interdye Distances between D and Cy Calculated from Anisotropy Data (R_a) as Well as Fluorescene Intensity (R_s) and Decay Time Data (R_t) Compared with Theoretical Values (R_{theo})

		$R_{D\text{-}Cy,theo}$ [a] (nm)		$R_{D\text{-}Cy,a}$ [b] (nm)			
sample no.	sample	μ	σ	μ	σ	$R_{D\text{-}Cy,t}$ [b] (nm)	$R_{D\text{-}Cy,s}$ [b,c] (nm)
A8/B1	D_1-Cy_2	6.4	0.6	6.6	0.3	5.1 ± 0.6	4.5 ± 0.7
A9/B1	D_1-Cy_1	4.1	0.7	4.0	0.3	4.8 ± 0.8	4.1 ± 0.8
A10/B1	D_2-Cy_2	7.4	0.7	7.3	0.3	5.4 ± 0.9	4.7 ± 0.7
A11/B1	D_2-Cy_1	6.4	0.6	6.6	0.3	5.2 ± 0.9	4.5 ± 0.7

[a]Calculated from AV-simulations. [b]With R_0(D-Cy) = 33.3 Å. [c]From ref 13.

IV. CONCLUSIONS

Specific interactions between ds-DNA and the dyes attached need to be fully characterized in order to obtain the correct desired information. Often the flexibility of the linker which attaches the dyes to the ds-DNA is a major factor limiting the interpretation of the experimental data. Especially, the analysis of molecular distances with the goal to monitor macromolecular conformational alterations often relies on the

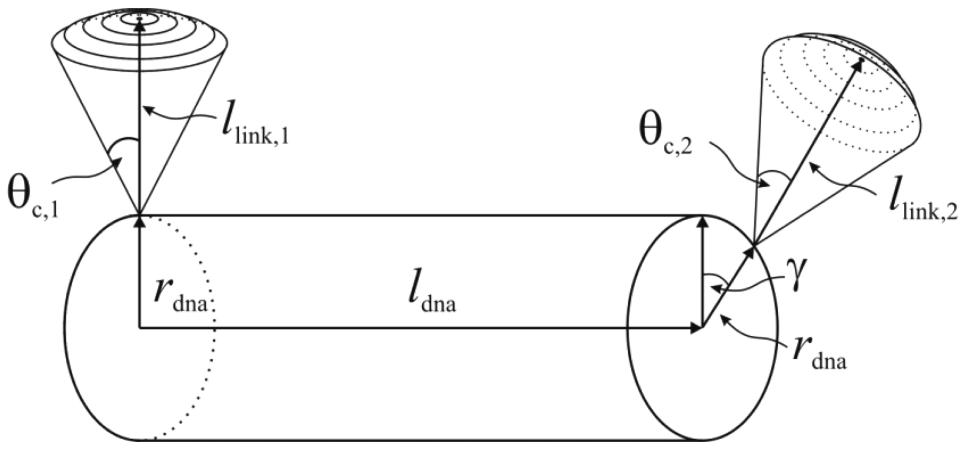

Figure 10. Scheme used for the calculation of an interdye distance distribution based on time-resolved anisotropy data.

dx.doi.org/10.1021/jp3064273 | J. Phys. Chem. B 2012, 116, 10798−10806

thorough analysis of FRET data. Knowledge on stiffness of the macromolecule as well as on the flexibility of the linker is therefore indispensible. However, for larger distances at which the energy transfer efficiencies are small the data evaluation becomes demanding and alternative approaches are needed. Here, complementary approaches to calculate the interdye distance between two chromophores using different experimental techniques and model applications were presented. Based on information on the mobility of the dyes, resulting from fluorescence decay time and fluorescence depolarization measurements, distributions for interdye distances were calculated. To make a comparison between these distances, the values from anisotropy measurements were in good agreement with those extracted from AV simulations for D and Cy. With the exception of the sample D_1-Cy_1 (**A9**/**B1**), all distances are close to the $2R_0$ limit of FRET. For such long distances, only very small transfer efficiencies are expected, which, consequently, will only induce minor alterations in the decay times of the dyes involved (see eqs 3 and 4) and, subsequently, the obtained distances are prone to larger uncertainties. Moreover, often the dye molecules used in standard FRET applications have fluorescence decay times in the same time regime (e.g., a few nanoseconds). The analysis of the corresponding fluorescence decay times with respect to distance distribution will be demanding in such cases since the observable differences maybe small which will induce a larger uncertainty in the analysis of the distance distribution (e.g., width of the distribution). The analysis of the anisotropy data is independent of FRET and, therefore, is not prone to such limitations, yielding better results (see Table 4) and may present a complementary view of the system under investigation. In the present case, the use of the Ru complex as a relay dye is proven to be very powerful, because the Ru complex has a luminescence decay time in the μs time regime, minimizing the above-mentioned difficulties even more. From the analysis of the Ru luminescence decays, the distance distributions were determined, which were consistent with the values from AV simulations. Moreover, the good agreement of the distance distribution parameters obtained by theoretical and experimental methods (time-resolved fluorescence and anisotropy) supports the use of the ds-DNA-distance model and the application of AV simulations as a fast but efficient way to estimate the corresponding parameters.

■ ASSOCIATED CONTENT

Supporting Information

Supporting figure and table. This material is available free of charge via the Internet at http://pubs.acs.org.

■ AUTHOR INFORMATION

Corresponding Author

*E-mail: kumke@uni-potsdam.de. Tel.: +49 331 977 5209. Fax: +49 331 977 5058.

Notes

The authors declare no competing financial interest.

■ REFERENCES

(1) Sapsford, Kim E.; Berti, Lorenzo; Medintz, Igor L. *Angew. Chem., Int. Ed.* **2006**, *45* (28), 4562−4589.
(2) Sahoo, H. *J. Photochem. Photobiol., C* **2011**, *12* (1), 20−30.
(3) Guo, J.; Ju, J.; Turro, N. *Anal. Bioanal. Chem.* **2012**, *402*, 3115−3125.
(4) Förster, T. *Ann. Phys.* **1948**, *437* (1), 55−75.
(5) Van der Meer, B. W.; Coker, G.; Simon Chen, S.-Y. *Resonance Energy Transfer: Theory and Data*; VCH: New York, 1994.
(6) Haustein, E.; Jahnz, M.; Schwille, P. *Chem. Phys. Chem.* **2003**, *4* (7), 745−748.
(7) Kawahara, S.; Uchimaru, T.; Murata, S. *Chem. Commun.* **1999**, 563−564.
(8) Watrob, H. M.; Pan, C.-P.; Barkley, M. D. *J. Am. Chem. Soc.* **2003**, *125* (24), 7336−7343.
(9) Jiang, Z.-J.; Goedel, W. A. *Phys. Chem. Chem. Phys.* **2008**, *10*, 4584−4593.
(10) Galperin, E.; Verkhusha, V. V.; Sorkin, A. *Nat. Methods* **2004**, *1* (3), 209−217.
(11) He, L.; Wu, X.; Simone, J.; Hewgill, D.; Lipsky, P. E. *Nucleic Acids Res.* **2005**, *33* (6), e61−e61.
(12) Kienzler, A.; Flehr, R.; Kramer, R. A.; Gehne, S.; Kumke, M. U.; Bannwarth, W. *Bioconjugate Chem.* **2011**, *22*, 1852−1863.
(13) Altevogt née Kienzler, A.; Flehr, R.; Gehne, S.; Kumke, M. U.; Bannwarth, W. *Helv. Chim. Acta* **2012**, *95* (4), 543−555.
(14) Stryer, L. *Annu. Rev. Biochem.* **1978**, *47*, 819−846.
(15) Lakowicz, J. R. *Principles of Fluorescence Spectroscopy*, 3rd ed.; Springer Verlag: New York, 2006.
(16) O'Connor, D. V.; Phillips, D. *Time-Correlated Single Photon Counting*; Academic Press: New York, 1984.
(17) Valeur, B. *Molecular Fluorescence − Principles and Applications*; Wiley-VCH: New York, 2002.
(18) Braslavsky, S. E.; Fron, E.; Rodriguez, H. B.; San Román, E.; Scholes, G. D.; Schweitzer, G.; Valeur, B.; Wirz, J. *Photochem. Photobiol. Sci.* **2008**, *7*, 1444−1448.
(19) Zachmann, H. G. *Mathematik für Chemiker*; Wiley-VCH: New York, 2007.
(20) Flehr, R.; Kienzler, A.; Bannwarth, W.; Kumke, M. U. *Bioconjugate Chem.* **2010**, *21*, 2347−2354.
(21) Luschtinetz, F.; Dosche, C.; Kumke, M. U. *Bioconjugate Chem.* **2009**, *20*, 576−583.
(22) Sindbert, S.; Kalinin, S.; Nguyen, H.; Kienzler, A.; Clima, L.; Bannwarth, W.; Appel, B.; Müller, S.; Seidel, C. A. M. *J. Am. Chem. Soc.* **2011**, *133* (8), 2463−2480.
(23) Sanborn, M. E.; Connolly, B. K.; Gurunathan, K.; Levitus, M. *J. Phys. Chem. B* **2007**, *111* (37), 11064−11074.
(24) Martí, A. A.; Puckett, C. A.; Dyer, J.; Stevens, N.; Jockusch, S.; Ju, J.; Barton, J. K.; Turro, N. J. *J. Am. Chem. Soc.* **2007**, *129* (28), 8680−8681.
(25) Muschielok, A.; Andrecka, J.; Jawhari, A.; Bruckner, F.; Cramer, P.; Michaelis, J. *Nat. Methods* **2008**, *5* (11), 965−971.
(26) Muschielok, A.; Michaelis, J. *J. Phys. Chem. B* **2011**, *115* (41), 11927−11937.
(27) Muschielok, A.; Michaelis, J. *FRETnps Tool*, Version 2.6; Ludwig-Maximilians-Universität Munich, Germany, 2008
(28) Case, D. A. et al. *AmberTools*, Version 1.4; University of California, San Francisco, U.S.A., 2010
(29) Seidel, C. A. M.; Schulz, A.; Sauer, M. H. M. *J. Phys. Chem.* **1996**, *100*, 5541−5553.
(30) Clegg, R. M.; Murchie, A. I.; Zechel, A.; Lilley, D. M. *Proc. Natl. Acad. Sci. U.S.A.* **1993**, *90* (7), 2994−2998.
(31) Clegg, R. M. *Methods Enzymol.* **1992**, *211*, 353−388.
(32) Hardin, R. H.; Sloane, N. J. A. *Proc. Symp. Appl. Math.* **1995**, *50*, 179−204.
(33) Hardin, R. H.; Sloane, N. J. A. Tables of Spherical Codes with Icosahedral Symmetry, published electronically at http://www2.research.att.com/~njas/icosahedral.codes/, 2000 (accessed on 27.04.2012).